IBRO Reports 6 (2019) 176–184

Contents lists available at ScienceDirect

IBRO Reports

journal homepage: www.elsevier.com/locate/ibror

Research Paper

Voltage-sensitive dye recording of glossopharyngeal nerve-related synaptic networks in the embryonic mouse brainstem

Yoko Momose-Sato[a], Katsushige Sato[b,*]

[a] Department of Nutrition and Dietetics, College of Nutrition, Kanto Gakuin University, Kanazawa-ku, Yokohama 236-8503, Japan
[b] Department of Health and Nutrition Sciences, Komazawa Women's University Faculty of Human Health, Inagi-shi, Tokyo 206-8511, Japan

ARTICLE INFO

Keywords:
Optical recording
Voltage-sensitive dye
Glossopharyngeal nerve
Synaptogenesis
Neural circuit formation
Development

ABSTRACT

The glossopharyngeal nerve (N.IX) transfers motor and sensory information related to visceral and somatic functions, such as salivary secretion, gustation and the control of blood pressure. N.IX-related neural circuits are indispensable for these essential functions. Compared with the strenuous analysis of morphogenesis, we are only just starting to elucidate the functiogenesis of these neural circuits during ontogenesis. In the present study, we applied voltage-sensitive dye recording to the embryonic mouse brainstem, and examined the functional development of the N.IX-related neural circuits. First, we optically identified the motor nucleus (the inferior salivatory nucleus (ISN)) and the first-order sensory nucleus (the nucleus of the tractus solitarius (NTS)). We also succeeded in recording optical responses in the second/higher-order sensory nuclei via the NTS, including the parabrachial nucleus. Second, we pursued neuronal excitability and the onset of synaptic function in the N.IX-related nuclei. The neurons in the ISN were excitable at least at E11, and functional synaptic transmission in the NTS was first expressed at E12. In the second/higher-order sensory nuclei, synaptic function emerged at around E12-13. Third, by mapping optical responses to N.IX and vagus nerve (N.X) stimulation, we showed that the distribution patterns of neural activity in the NTS were different between the N.IX and the N.X from the early stage of ontogenesis. We discuss N.IX-related neural circuit formation in the brainstem, in comparison with our previous results obtained from chick and rat embryos.

1. Introduction

The glossopharyngeal nerve (N.IX) is one of the multi-functional cranial nerves. The N.IX contains special and general visceral efferent fibers, special and general visceral afferent fibers, and general somatic afferent fibers (Carpenter, 1985; Kandel et al., 2013; Sajgo et al., 2016). The N.IX is related to many essential functions, such as salivary secretion, gustation and the control of blood pressure. In vertebrates, morphological and genetic investigations have disclosed the structures of motor and sensory nuclei in the brainstem and the neural circuits from/to the higher brain (Norgen and Leonard, 1973; Norgen, 1978; Travers, 1988; Whitehead, 1990, 1993; Beckmann and Whitehead, 1991; Zaidi et al., 2008). Ontogenetically, it is demonstrated that branchiomotor and visceromotor neurons of the N.IX originate within rhombomere 6 (Simon and Lumsden, 1993; Watari et al., 2001), and that combinations of transcription factors regulate the development of neural circuits in the brainstem (Chambers et al., 2009; Chédotal and Rijli, 2009; Sajgo et al., 2016). However, the functional development of N.IX-related pathways is still not fully understood, because of technical limitations in monitoring electrical activity from small and fragile neurons in the developing central nervous system (CNS).

In order to surmount these obstacles, we have applied voltage-sensitive dye (VSD) recording with a multi-element photodiode array to the embryonic CNS, especially the brainstem (for reviews see Momose-Sato et al., 2001, 2002, 2015; Momose-Sato and Sato, 2006, 2011). This technique has been developed and used to investigate the spatio-temporal dynamics of neural activity in a variety of invertebrate and vertebrate CNSs (for reviews see Cohen and Salzberg, 1978; Salzberg, 1983; Grinvald et al., 1988; Ebner and Chen, 1995; Baker et al., 2005; Canepari et al., 2015). In our previous studies, we proved its usefulness

Abbreviations: APV, DL-2-amino-5-phosphonovaleric acid; CNQX, 6-cyano-7- nitroquinoxaline-2,3-dione; CNS, central nervous system; EPSP, excitatory postsynaptic potential; ISN, inferior salivatory nucleus; N.IX, glossopharyngeal nerve; N.X, vagus nerve; NTS, nucleus of the tractus solitarius; PBN, parabrachial nucleus; VSD, voltage-sensitive dye

* Corresponding author at: Department of Health and Nutrition Sciences, Komazawa Women's University Faculty of Human Health, 238 Sakahama, Inagi-shi, Tokyo 206-8511, Japan.
E-mail address: katsu-satoh@komajo.ac.jp (K. Sato).

https://doi.org/10.1016/j.ibror.2019.05.004
Received 14 March 2019; Accepted 13 May 2019

in the field of developmental neuroscience (for reviews see Momose-Sato et al., 2001, 2015; Glover et al., 2008; Sato and Momose-Sato, 2017).

Concerning the N.IX-related nuclei and neural circuits in the brainstem, we have examined spatiotemporal patterns and the developmental dynamics of neural activity in the embryonic chick and rat brainstems (Sato et al., 1995, 2002a,b; Sato and Momose-Sato, 2004a, b; Momose-Sato et al., 2007, 2011). In chick embryos, we succeeded in detecting neural activity in the N.IX-related motor nucleus and the first-order sensory nucleus, the nucleus of the tractus solitarius (NTS), and identified the developmental origins of neural excitability and synaptic function. We also examined the similarities and differences in optical responses between the N.IX and the vagus nerve (N.X) in chick and rat embryos (Sato et al., 1995, 2002b; Momose-Sato et al., 2011).

In the present study, we extended the subject of study to the mouse embryo. The first goal of the present study was to optically identify the N.IX-related motor and sensory nuclei in the mouse brainstem. The second aim was to survey the second/higher-order sensory nuclei, and examine functional development of neural circuits associated with these nuclei. The third purpose was to compare the optical response patterns of N.IX-related neural circuits with those of the N.X reported previously (Momose-Sato and Sato, 2016).

2. Materials and methods

2.1. Preparations

Experiments were carried out in accordance with the Japan Society for the Promotion of Science guidelines and the National Institutes of Health guidelines for the care and use of laboratory animals, with the approval of the Ethics Committee of Kanto Gakuin University and Komazawa Women's University. All efforts were made to minimize the number of animals used and their suffering. ICR mice at 11–14 days gestation (E11-E14) (Nippon Bio-Supp. Center, Tokyo, Japan) were used. Females were caged with males in the evening and checked for sperm the next morning: this day was termed E0. Pregnant mice were anesthetized with ether, and the spinal cord was dislocated at the cervical level. Their fetuses were then surgically removed and decapitated in an ice-cold solution. The brainstem preparation with the N.IX (and the N.X in some cases) attached (n = 3 at E11, n = 4 at E12, n = 6 at E13, n = 14 at E14) was dissected under a dissecting microscope. For *en bloc* preparations, the dorsal midline of the cerebellum and midbrain was cut, and the preparation was flattened by bilaterally reflecting the cerebellum. Slice preparations of about 900 − 1400 μm were made from the isolated brainstem at the level of the N.IX/N.X root. Transection was performed using a hand-held blade. The early embryonic brain had a histologically loose structure with immature neurons and undifferentiated connective tissue, and was relatively resistant to anoxia. Therefore, a whole brainstem preparation was available *in vitro*, which made it possible to investigate the functional organization of neural networks in the brainstem. The preparations were kept in artificial cerebrospinal fluid (ACSF) that contained (in mM) NaCl, 124; KCl, 5; $CaCl_2$, 2.5; $MgSO_4$, 1; NaH_2PO_4, 1.25; $NaHCO_3$, 22; and glucose, 10, equilibrated with a mixture of 95% O_2 and 5% CO_2 (pH 7.4), or in Ringer's solution that contained (in mM) NaCl, 149; KCl, 5.4; $CaCl_2$, 1.8; $MgCl_2$, 0.5; glucose, 10; and Tris-HCl buffer (pH 7.4), 10 equilibrated with oxygen.

2.2. Staining with a voltage-sensitive dye (VSD)

There has been great progress in the development of VSDs for the measurement of rapid changes in membrane potential (for reviews, see Dasheiff, 1988; Loew, 1988; Ebner and Chen, 1995; Tsytsarev et al., 2014; Miller, 2016). The high translucency of embryonic tissues causes large signal-to-noise ratios in absorption measurements. Therefore, absorption rather than fluorescent VSDs perform better in embryonic preparations (Momose-Sato et al., 2001; Mullah et al., 2013). Of the VSDs tested thus far, a merocyanine-rhodanine absorption dye, NK2761 (Hayashibara Biochemical Laboratories Inc./Kankoh-Shikiso Kenkyusho, Okayama, Japan: Kamino et al., 1981; Salzberg et al., 1983), was demonstrated to be the best for embryonic nervous and cardiac tissues (Kamino, 1991; Momose-Sato et al., 1995; Mullah et al., 2013). Thus, we used this dye in the present experiment. The meningeal tissue surrounding the isolated brain was carefully removed in a bathing solution under a dissection microscope, and the preparation was stained by incubation for 10–15 min in a solution containing 0.2 mg/ml of NK2761. The immature cellular-interstitial structure of the embryonic tissue allowed the dye to diffuse well from the surface into deeper regions. After the staining, each preparation was attached to the silicone bottom of a recording chamber with the ventral side up for *en bloc* preparations, or with the caudal side up for slice preparations, by pinning with tungsten wires. The preparation was continuously superfused with the bathing solution at 2–3 ml/min at room temperature, 24–28 °C.

2.3. Electrical stimulation of the N.IX/N.X

To evoke neural responses in the glossopharyngeal and vagal nuclei, the N.IX or the N.X was stimulated with a glass microsuction electrode (about 50–100 μm internal diameter). Positive (depolarizing) square current pulses (20–40 μA/1 msec for E11 and 8 μA/5 msec for E12-14), which evoked the maximum response, were applied to the N.IX or the N.X with a single shot or with two shots at an interval of 30 s.

2.4. Blocker experiments

To examine the pharmacological nature of the postsynaptic response, the following drugs were used: DL-2-amino-5-phosphonovaleric acid (APV) was acquired from Sigma Chemical Co. (St. Louis, MO, USA), and 6-cyano-7-nitroquinoxaline-2,3-dione (CNQX) was acquired from Research Biochemicals International (Natic, MA, USA). The effects of the blocker were evaluated 10–15 min after application of the drug.

2.5. Optical recording with a voltage-sensitive dye

Bright-field illumination was provided by a 300 W tungsten-halogen lamp (Type JC-24 V/300 W, Kondo Philips Ltd., Tokyo, Japan) driven by a stable DC-power supply, and incident light was collimated and rendered quasi-monochromatic using an interference filter with a transmission maximum at 699 ± 13 nm (half-width) (Asahi Spectra Co., Tokyo, Japan). The objective (Plan Apo, ×4: 0.2 NA and x10: 0.4 NA) and photographic eyepiece (×2.5) lenses projected a real image of the preparation onto a 34 × 34-element silicon photodiode matrix array mounted on a microscope. The focus was set to the surface of the preparation, but the optical signals seemed to include activity from every depth, since it was previously shown that the loose cellular-interstitial structure of the embryonic tissue allows the dye to diffuse readily from the surface to deeper regions and consequently stain neurons relatively well (Sato et al., 1995), and that neural responses in the dorsally-located cranial nerve nucleus could be detected from the ventral surface (Momose-Sato et al., 1991). Changes in the transmitted light intensity through the preparation were detected with the photodiode array and recorded with a 1020-site optical recording system constructed in our laboratory. This system is based on one described previously (Hirota et al., 1995; Momose-Sato et al., 2001, 2015) with modifications to its analog-to-digital converter unit. Each pixel (element) of the photodiode array detected light transmitted by a square region (116 × 116 μm^2 using ×10 magnification and 46 × 46 μm^2 using ×25 magnification) of the preparation. The outputs from the 1020 elements of the photodiode array were fed into individual current-to-voltage converters followed by individual pre-amplifiers. The AC component of each signal was further amplified (time constant of AC

coupling = 3 s), passed through an RC low-pass filter (time constant = 470 μsec), digitized with a 16-bit dynamic range, and sampled at 1024 Hz. This system makes it possible to detect optical signals without the drift in the DC baseline that is associated with dye bleaching.

2.6. Data analysis

The fractional change in dye absorption $\Delta A/A_r$ is equal to $-\Delta I/(I_{before\ staining}-I_{after\ staining})$, where I is the light intensity transmitted through the preparation (Ross et al., 1977). In most of our experiments, we had already stained the preparation before placing it in the recording chamber. This was done to maximize the diffusion of the dye into the tissue, but it prevented us from measuring $I_{before\ staining}$ and $I_{after\ staining}$ in the same preparation. When we compared $I_{before\ staining}$ and $I_{after\ staining}$ in chick brainstems stained on the microscope's stage, the regional variation in $I_{after\ staining}/I_{before\ staining}$ was small (Momose-Sato and Sato, 2006). Assuming that the conditions were similar between the chick and mouse embryos, we measured $I_{after\ staining}$ and ΔI, and expressed the optical signal as $\Delta I/I_{after\ staining}$ in the present study. Color-coded representations of the optical signals to be used in the spatio-temporal activity map were constructed using the "NeuroPlex" program (RedShirtImaging LLC, Fairfield, CT, USA). The color coding in the figures is linearly distributed between the minimum and maximum values of ΔI/I.

3. Results

3.1. Optical identification of N.IX-related nuclei in the E12 mouse brainstem

Fig. 1A illustrates multiple-site optical responses induced by N.IX stimulation in an E12 mouse brainstem *en bloc* preparation. The signals were detected using a 34 × 34-element photodiode array, and those on the stimulated side are shown. N.IX stimulation elicited optical responses in two regions, i.e., a rostro-medial region (indicated by gray shadow) and a lateral region located longitudinally in the rostro-caudal direction.

Fig. 1B shows enlarged optical signals detected in these two regions. The signals detected in the rostro-medial region (positions 1 and 2) consisted of a fast spike-like signal (indicated by arrowheads), whereas those in the lateral region (positions 3 and 4) exhibited two components: a fast spike-like signal (indicated by arrowheads) and a long-lasting slow signal (indicated by asterisks). The direction and size of the fast and slow signals were dependent on the wavelength of the incident light (data not shown), which is consistent with the action spectrum of the merocyanine-rhodanine dye, NK2761 (Momose-Sato et al., 1995). The result confirmed that the fast and slow signals represented dye-absorption changes related to the membrane potential.

Fig. 2A demonstrates the optical signals induced by N.IX stimulation in an E12 mouse brainstem slice preparation. Optical signals consisting of the fast and slow components were observed in the dorso-lateral region. The spike-like signals near the N.IX root were electrotonic responses because the direction of the signals was reversed with hyperpolarizing current pulse stimulation (data not shown). The fast signals identified in the shadowed region in Fig. 1A were not detected in Fig. 2A because the rostral medulla was cut and not included in this preparation.

Enlarged optical signals detected in the dorso-lateral region (indicated by an asterisk in Fig. 2A) are shown in Fig. 2B. The slow signal was completely eliminated in the Ca^{2+}-free or Cd^{2+} (100 μM)-containing solution (data not shown) and with application of glutamate receptor antagonists, APV (200 μM) and CNQX (5 μM) (Fig. 2B). These results suggest that the slow signal corresponds to the glutamatergic excitatory postsynaptic potential (EPSP), while the fast signal is associated with the action potential, as has been demonstrated for other cranial nerve nuclei (Momose-Sato et al., 2001, 2015).

The mouse N.IX bundle contains motor and sensory fibers, so that electrical stimulation to the N.IX bundle elicits neural responses in both the motor and sensory nuclei. Compared with anatomical data (Jacobowitz and Addott, 1997; Schambra, 2008; Watson et al., 2012), it is reasonable to consider that (1) the gray-shadowed region (Fig. 1A) with the fast signal alone corresponds to the motor nucleus of the N.IX, possibly the inferior salivatory nucleus (ISN), and that (2) the dorso-lateral region (Figs. 1A and 2 A), in which both the fast and slow signals were detected, corresponds to the sensory nucleus, the nucleus of the tractus solitarius (NTS). The action potential in the motor nucleus was also detected from E11 preparations (data not shown), suggesting that motoneuronal excitability was generated at least at E11.

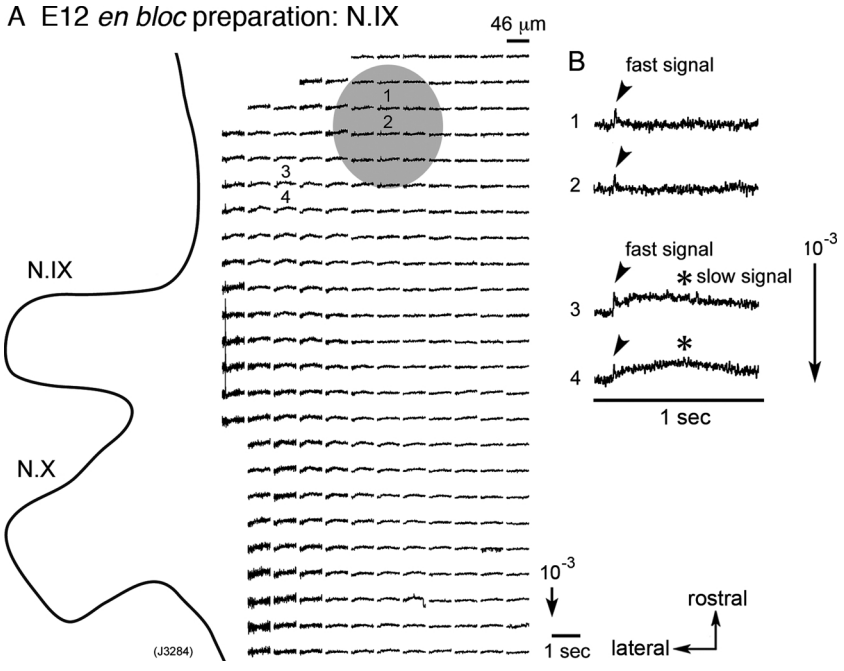

Fig. 1. (A) Optical recording of neural responses to N.IX stimulation in an E12 mouse *en bloc* preparation. The recording was made with the ventral side up and with a magnification of x25. The cut end of the N.IX was electrically stimulated with a depolarizing pulse (8 μA/5 msec) using a suction electrode. The relative position of the image of the preparation is drawn on the recording, and signals detected on the stimulated side are shown. The direction of the arrow in the lower right of the figure indicates an increase in transmitted light intensity (a decrease in dye absorption), and the length of the arrow represents the stated value of the fractional change. (B) Enlarged traces of optical signals detected in positions 1–4 in A. The signals detected in the rostro-medial region (gray shadow: positions 1 and 2) consisted of a fast spike-like signal (indicated by arrowheads), whereas those detected in the lateral region (positions 3 and 4) exhibited two components: a fast spike-like signal (indicated by arrowheads) and a long-lasting slow signal (indicated by asterisks). In this and other recordings, signal averaging of two trials was performed offline. N.IX, glossopharyngeal nerve; N.X, vagus nerve.

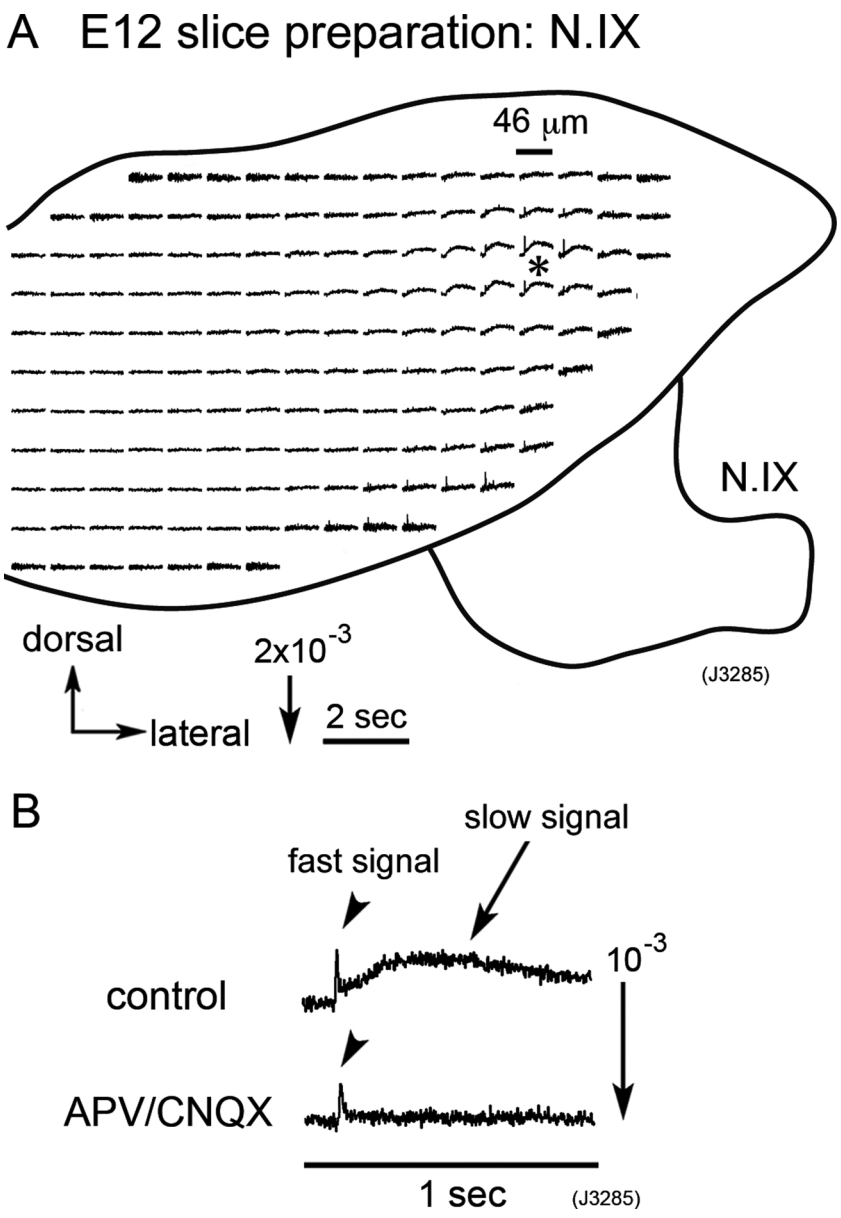

Fig. 2. (A) Optical recording of neural responses to N.IX stimulation in an E12 mouse medulla slice preparation. The recording was made with the caudal side up. The fast signals observed near the root of the N.IX were reversed in polarity with hyperpolarizing stimulation (data not shown), suggesting that they were not active responses but electrotonic potentials. (B) Enlarged traces of optical signals detected in the dorsolateral region (a position indicated by an asterisk in A). The upper trace is a signal detected in a physiological solution, and the lower trace is a signal in a solution containing both APV (200 μM) and CNQX (5 μM). The slow signal was eliminated in the presence of these glutamate receptor antagonists.

3.2. Optical detection of N.IX-related synaptic networks in the brainstem

Next, we pursued N.IX-related synaptic networks in the embryonic mouse brainstem, and compared them with N.X-related synaptic networks. For this purpose, we detected optical responses from a wider region of the brainstem with a lower magnification (x10) of the microscope.

Fig. 3A and B show examples of multiple-site optical recording of neural activity evoked by N.IX (A) and N.X (B) stimulation in an E14 *en bloc* brainstem preparation. When the N.IX was stimulated (Fig. 3A), in addition to the responses in the caudal medulla (Area 1: pink shadow), other response areas were identified in the rostral medulla (Area 2: orange shadow) and pons (Area 3: green shadow) on the ipsilateral side. In these areas, the optical signals contained the slow component. The small slow signals were also observed in some positions on the contralateral side (as indicated by arrowheads). In Fig. 3A, the motor nucleus of the N.IX, in which only the fast signal should be detected, was not clearly identified. This was probably because the signal size and the area of the motor nucleus were so small that the nucleus could not be distinguished with the lower magnification.

As shown in Fig. 3B, N.X stimulation also produced the slow signals in Areas 1–3 on the ipsilateral side (pink, orange and green shadows) and in some positions on the contralateral side (as indicated by arrowheads). The response pattern was very similar to that with N.IX stimulation (Fig. 3A), although there were some differences in the details (see a later section referring to Figs. 5 and 6).

Fig. 4 compares the onset timings of optical signals induced by N.IX stimulation in Areas 1–3 and on the contralateral side. The signals detected in Areas 2 and 3 and on the contralateral side showed significant delays compared with the signal detected in Area 1. Similar delays were also observed with N.X stimulation (Momose-Sato and Sato, 2016). These delays were considered to reflect signal propagation along the polysynaptic pathway. This result suggests that Area 1 corresponds to the first-order sensory nucleus, the NTS, and the other areas to the second- or higher-order nucleus of the N.IX/N.X pathway, which receives polysynaptic inputs via the NTS.

3.3. Contour line maps of the slow signal

To examine the spatial distribution patterns of the optical signal in more detail, we measured the slow signal amplitudes and constructed contour line maps. Typical examples are shown in Fig. 5, which

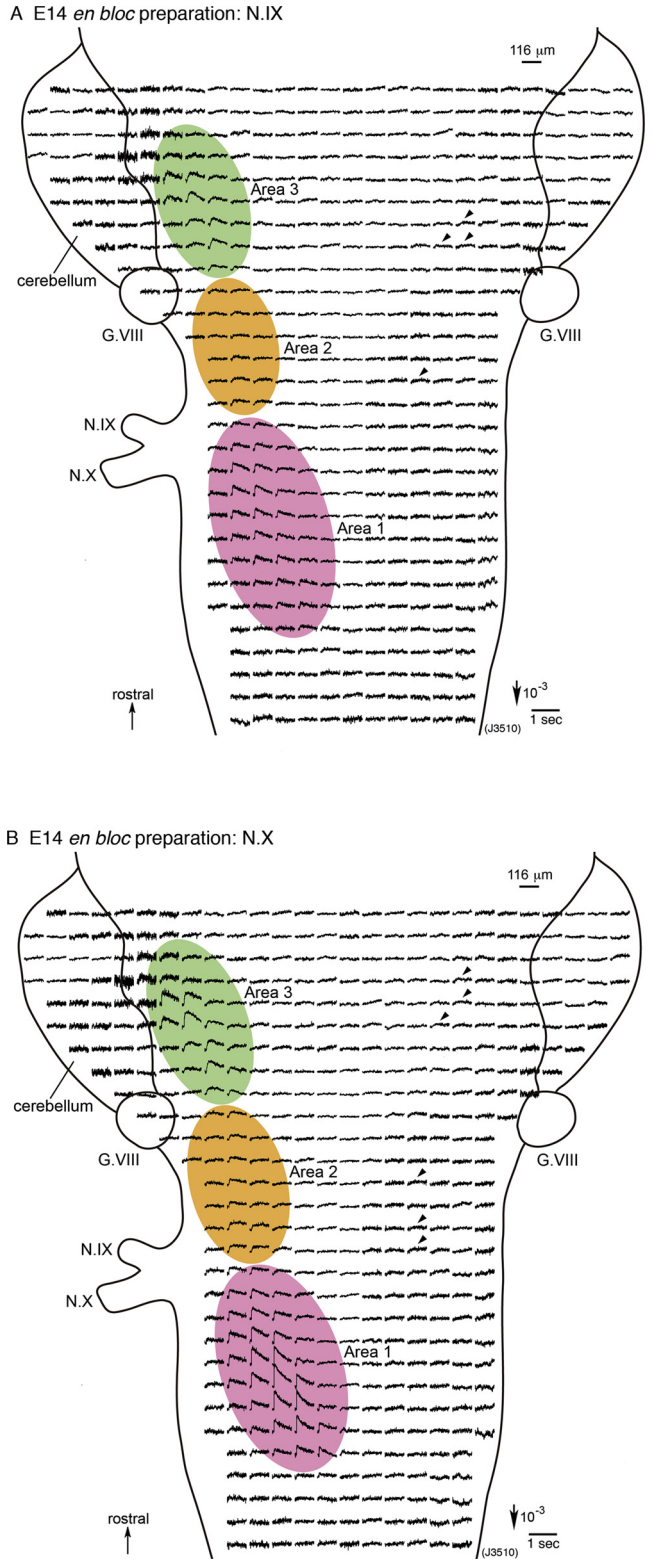

Fig. 3. 1020-site optical recordings of neural responses to N.IX (A) and N.X (B) stimulation in an E14 mouse brainstem *en bloc* preparation. The recordings were made with a magnification of x10 to detect optical responses from a wide region of the brainstem. Either N.IX or N.X stimulation elicited neural responses in three areas (Areas 1–3) on the stimulated side. Area 1 (pink shadow) was located at the caudal level of the N.IX/N.X root, and corresponded to the NTS. Areas 2 and 3 (orange and green shadows, respectively) were discerned in the rostral medulla and pons, respectively. On the contralateral side, small slow signals were detected in several positions as typified by arrowheads. The colored-response areas were determined by eye, whereas the precise maps are shown in Fig. 5B. G.VIII, vestibulo-cochlear ganglion.

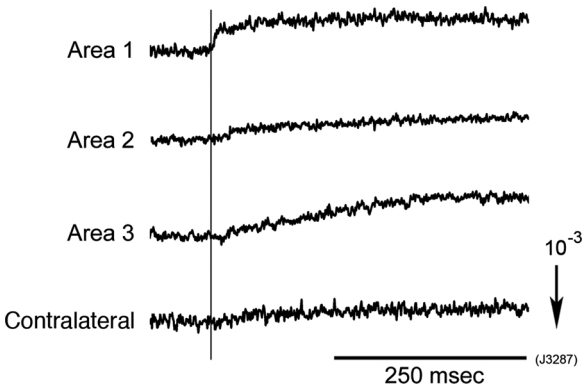

Fig. 4. Enlarged traces of the N.IX-related optical signals recorded from Areas 1–3 and the contralateral side of an E14 *en bloc* brainstem. The vertical line indicates the onset timing of the signal in Area 1. Significant delays of the onsets existed between the signal in Area 1 and the signals in other areas. This suggests that the latter signals correspond to polysynaptic responses in the second/higher-order nuclei.

represents maps made from an E13 (A) and E14 (B) *en bloc* preparation for the N.IX (left) and the N.X (right). In these maps, the slow signals were distributed in a layered pattern surrounding some peaks. Peak locations and response areas ($\Delta I/I \geq 1.0 \times 10^{-4}$) were extracted from the contour line maps and are shown in Fig. 6. In Fig. 6, data of case 2 and case 3 were obtained from the preparations shown in Fig. 5, and case 1 is another example at E13. Peak locations are shown with filled circles, and response areas are illustrated with lines (N.IX: blue, N.X: red).

From the maps shown in Figs. 5 and 6, the following characteristics were extracted: (1) As provisionally observed in Fig. 3, the slow signal area on the ipsilateral side was divided into Areas 1–3 according to the distribution pattern. (2) On the contralateral side, small response areas of slow signals were identified, which seemed to be located symmetrically to Areas 2 and 3. (3) The contour line exhibited a single peak in each area except for Area 3, in which two peaks were usually observed. (4) The distribution patterns of the N.IX and the N.X were very similar, but a difference was observed in Area 1 (NTS): the area and peak location of the N.X were caudally deviated to those of the N.IX in many preparations (e.g., case 1 and case 3 in Fig. 6).

In optical recording with the VSD, it is assumed that the fractional change ($\Delta A/A$) is proportional to the magnitude of the membrane potential changes in each cell and process, and to the number and membrane area of activated (excitable) neural elements within the field detected optically by one photodiode under conditions in which the amount of dye bound to the membrane is uniform (Obaid et al., 1985; Orbach et al., 1985). In the present study, it can be reasonably assumed that $\Delta I/I$ is linearly related to $\Delta A/A$ (see Materials and methods). Thus, the spatial distribution of the slow signal shown in Figs. 5 and 6 reflects spatial distributions of synaptic function, and the peak location of the EPSP amplitude represents the region with the highest activity and/or number of neurons that produced the EPSP. The functional organization of the N.IX- and N.X-related nuclei described above, especially that indicated in (3) and (4), will be addressed in the Discussion section.

3.4. Development of N.IX-related synaptic networks in the brainstem

To investigate the development of N.IX-related synaptic pathways in the brainstem, we examined the appearance of the slow signals in Areas 1–3 and on the contralateral side at E11-E14 (Table 1). The results showed that (1) functional synaptic transmission in the NTS (Area 1) was first expressed at E12, and that (2) polysynaptic responses were detected in Areas 2 and 3 from E12-E13, and in the contralateral region from E13-14. These findings suggest that polysynaptic responses appear within a day after the initial expression of EPSPs in the first relay

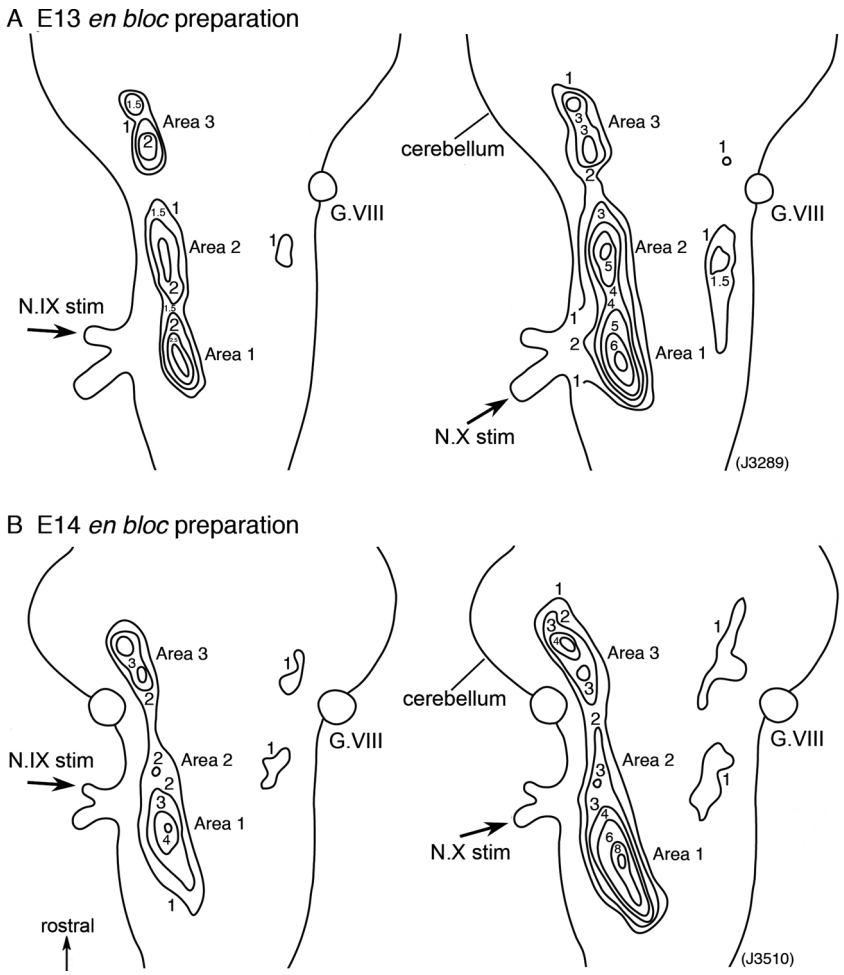

Fig. 5. Contour line maps of the amplitude of the slow signal in response to N.IX (left panels) and N.X (right panels) stimulation in an E13 (A) and E14 (B) *en bloc* brainstem preparation. The numerals on the contour lines indicate the fractional change multiplied by 10^4. Maps in B were obtained from the preparation shown in Fig. 3.

nucleus, the NTS.

4. Discussion

In the present study, we detected optical responses induced by N.IX stimulation in the embryonic mouse brainstem, and surveyed developmental changes in response patterns during ontogenesis. In our previous papers (Sato et al., 1995, 2002a, 2002b; Sato and Momose-Sato, 2004a, b; Momose-Sato et al., 2007, 2011), we succeeded in monitoring N.IX- and N.X-related optical responses in chick and rat embryonic brainstems. In the following sections, we compare and discuss the developmental dynamics of N.IX-pathway formation between species.

4.1. Optical identification of the N.IX-related motor and first-order sensory nuclei

In the E12 preparation (Figs. 1A and 2 A), only the fast spike-like signal (corresponding to the action potential) was observed in the rostro-medial region, whereas the slow signal (corresponding to the EPSP) following the fast signal was detected in the dorso-lateral region. By comparing with anatomical information (Jacobowitz and Addott, 1997; Schambra, 2008; Watson et al., 2012), we concluded that these regions correspond to the motor and sensory nuclei of the N.IX, respectively. Similar response patterns were observed in the embryonic chick (Sato et al., 1995, 2002a,b; Sato and Momose-Sato, 2004a, b; Momose-Sato et al., 2007) and rat (Momose-Sato et al., 2011) brainstems, suggesting that the essential nature of nuclear organization is conserved between species.

Concerning the motor nucleus of the N.IX, different nomenclatures have been used in different species. In the chick, Breazile (1979) referred to the motor nucleus as "the nucleus of the glossopharyngeal nerve". Altman and Bayer (1980, 1982) used the term "the retrofacial nucleus". According to textbook descriptions (Carpenter, 1985; Watson et al., 2012; Kandel et al., 2013), the motoneurons of the N.IX form a cluster called the inferior salivatory nucleus (ISN). Some motoneurons are also contained in the nucleus ambiguus (Carpenter, 1985; Kandel et al., 2013), although the major contributor to this nucleus is considered to be the N.X (Altman and Bayer, 1980). In our optical recording, neuronal responses in the nucleus ambiguus were not identified in the early embryos even with N.X stimulation (Sato et al., 1998; Momose-Sato and Sato, 2016). Based on these considerations, we refer to the motoneuronal area of the N.IX as the ISN in the present study.

The action potential in the ISN was detected from E11, the earliest stage examined in the present study. Abadie et al. (2000) reported spontaneous neuronal activity from the mouse N.IX bundle at 10.5 days post coitus, suggesting that motoneurons are already functional at this stage. Action potentials of the N.IX motoneuron have been detected as early as E3.5 in chick embryos (Momose-Sato et al., 2007) and at least at E13 in rat embryos (Momose-Sato et al., 2011). The gross morphology of E10.5 mice corresponds to that of E12.5 rats and stage 23 (E3.5-E4) chick embryos (Sissman, 1970). Thus, excitability of

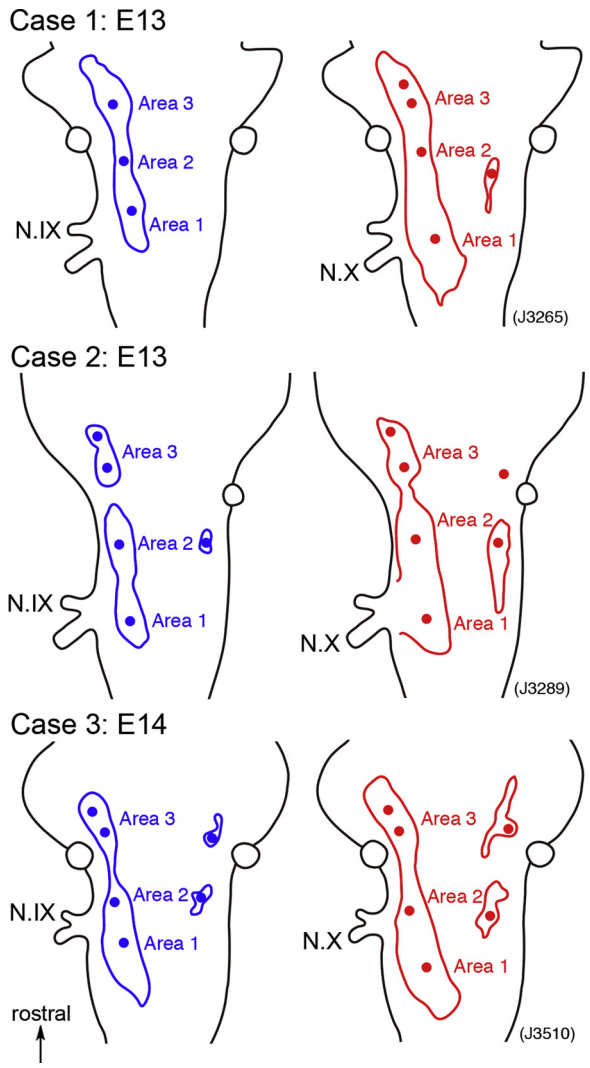

Fig. 6. Typical examples of the slow signal area and the peak locations of the slow signal amplitude. Cases 1 and 2 were obtained from E13 preparations, and case 3 was obtained from an E14 preparation. The slow signal areas ($\Delta I/I \geq 1.0 \times 10^{-4}$) are illustrated with lines, and locations of the peak are shown with filled circles. Blue lines and circles correspond to N.IX responses, and red ones to N.X responses.

motoneurons may be expressed at similar developmental stages in different species.

4.2. Development of synaptic transmission in the NTS

In the sensory nucleus of the N.IX, the NTS, the EPSP was mediated by glutamate (Fig. 2B), which was similar to the N.X (Momose-Sato and Sato, 2016), and to chick (Komuro et al., 1991; Momose-Sato et al., 1994; Sato et al., 1995) and rat (Sato et al., 1998; Momose-Sato et al., 2011) embryos. N.IX stimulation induced the EPSP signal from E12 (Table 1), showing that synaptic transmission is functional at this stage. In our previous study (Momose-Sato and Sato, 2016), the EPSP was evoked with N.X stimulation from E11-E12. In the chick embryo, the EPSP was initially expressed at E6-E7 in the N.IX- and N.X-related NTS (Momose-Sato et al., 1994; Sato and Momose-Sato, 2004a). In the case of rats, the EPSP initially emerged at E15 in the N.IX- and N.X-related NTS in normal physiological solution (Sato et al., 1998; Momose-Sato et al., 2011). Considering that the EPSP of the N.IX was smaller in amplitude than that of the N.X, and thus was less detectable using our criteria (significant when $\Delta I/I \geq 1.0 \times 10^{-4}$), it seems likely that functional synaptic transmissions of the N.IX and the N.X emerge almost at the same developmental stage.

Table 1
Expression of EPSPs in the N.IX-related sensory pathway.

		Area 1 (NTS)	Area 2 (rostral medulla)	Area 3 (pons)	Contralateral region
E11	J3269	−	−	−	−
	J3270	−	−	−	−
E12	J3282	+	−	−	−
	J3284	±	±	±	−
E13	J3288	±	−	±	−
	J3265	+	+	+	−
	J3287	+	+	+	±
	J3289	+	+	+	±
E14	J3357	+	−	+	−
	J3510	+	+	+	±
	J3345	+	+	+	+

The first and second columns give the embryonic day and the preparation references, respectively. The third to sixth columns show the appearance of the slow signal in Areas 1–3 and the contralateral region. "−" shows that no significant optical signal was detected ($\Delta I/I < 1 \times 10^{-4}$), "±" means that the maximum signal amplitude was $\geq 1 \times 10^{-4}$ and $< 2 \times 10^{-4}$, and "+" indicates that distinct optical signals ($\Delta I/I \geq 2 \times 10^{-4}$) were identified with a regional peak in each area.

4.3. Optical survey of N.IX-related polysynaptic pathways in the brainstem

Our optical survey with low magnification (Fig. 3) identified postsynaptic responses in several regions other than the NTS. The existence of delays in signal onsets (Fig. 4) suggested that the responses in Areas 2 and 3 and those on the contralateral side corresponded to the neural activity in second/higher-order nuclei of the N.IX pathway.

It is known that the major target for projections directly from the NTS (Area 1) is the parabrachial nucleus (PBN), which is located on the dorsolateral region of the pons (Norgen, 1978; Herbert et al., 1990; Watson et al., 2012). By comparing with anatomical information (Jacobowitz and Addott, 1997; Schambra, 2008; Watson et al., 2012), it is most likely that Area 3 in the present study corresponds to the PBN. In the map shown in Figs. 5 and 6, multiple peaks were observed in Area 3, while other areas usually exhibited single peaks of signal amplitudes. From this result, we cannot exclude the possibility that Area 3 does not correspond to a single nucleus but is composed of two nuclei that overlap ventrodorsally. Another possibility is that the PBN is consisted of multiple cores/subnuclei at the early stage of development. Optical studies in chick and rat embryos demonstrated that the motor nucleus of the N.IX and the N.X exhibited multiple cores at the initial stage of functional organization, and that the cores fuse with each other to form a single peak as development proceeded (Sato et al., 2002b; Momose-Sato et al., 2011). Similar changes in functional organization might be present in the PBN.

The structural basis of Area 2 is unclear at present. Possible candidates are the parvicellular reticular formation, the motor nucleus of the trigeminal, facial, vagal, and hypoglossal nerves, and the rostral ventrolateral medulla (RVLM) including the A1 noradrenergic cell group (Norgen and Leonard, 1973; Norgen, 1978; Watson et al., 2012). It is possible that Area 2 is an integration of several of the regions listed above.

The contralateral response areas were symmetrically located to ipsilateral Areas 2 and 3, suggesting that they correspond to the contralateral versions of Areas 2 and 3. If this is the case, it seems likely that projection from the NTS to higher centers of the N.IX/N.X is bilateral even though the major pathway is ipsilateral. Similar projection patterns have also been observed in rat embryos (Momose-Sato et al., 2013), but not in chicks, in which the projection from the NTS to the PBN was only contralateral (Sato et al., 2004).

4.4. Development of N.IX-related polysynaptic pathways

As shown in Table 1, N.IX-related polysynaptic responses in Areas 2 and 3 were detected from E12-13. In the case of the N.X (Momose-Sato and Sato, 2016), initial appearances of polysynaptic EPSPs were at E12-13 in Area 2 and at E12 in Area 3. These results suggest that synaptic function in the higher-order nuclei, especially the PBN (Area 3), is already generated within one day after synaptic function in the first relay nucleus (the NTS: Area 1) is initially expressed (E12 with the N.IX and E11-12 with the N.X).

Polysynaptic responses on the contralateral side were not significant before E13, and expressed one day later than the emergence of polysynaptic responses on the ipsilateral side. One possible explanation is that ipsilateral ascending pathway develops earlier than the contralateral ascending pathway, although we cannot exclude the possibility that small, undetectable EPSPs were present on the contralateral side as early as E12.

In chick embryos, polysynaptic vagal responses in the PBN were first detected from E7 (Sato et al., 2004), while synaptic transmission in the NTS was initially expressed at E6-E7 (Momose-Sato et al., 1994). This result suggests that the chronological sequence of neural network formation is similar between species. A short time lag of synaptic expression between the NTS and higher centers suggests that neural networks do not sequentially develop from the periphery to higher centers, but are formed independently of presynaptic innervation.

4.5. Comparison of the nuclear organization of the N.IX and the N.X

The spatial distributions of the slow signals shown in Figs. 5 and 6 reflect spatial distributions of synaptic function, and the peak locations of the EPSP amplitude represent the regions with the highest activity and/or number of neurons that produced the EPSP. As shown in Fig. 6, although the response areas of the N.IX and the N.X largely overlapped, the peak position and area of the N.X-related NTS (Area 1) were caudally deviated to those of the N.IX-related NTS. Similar results were also observed in the embryonic chick (Sato et al., 1995; Sato and Momose-Sato, 2004b) and rat (Momose-Sato et al., 2011) NTS. These results suggest that there is a viscerotopic organization within the NTS from the early stage of ontogenesis.

Even in the preparation with a different spatial distribution of the NTS (Area 1), responses in the PBN (Area 3) were similar between the N.IX and the N.X. (e.g. Fig. 3). Visceral information conducted by the N.IX and the N.X is simultaneously processed and integrated in the NTS (Mifflin and Felder, 1990; Paton and Kasparov, 2000). Experiments performed in chick embryos demonstrated the convergence of peripheral inputs via the N.IX and the N.X at the level of the NTS (Sato and Momose-Sato, 2004b). Further investigations are necessary to conclude whether similar convergence is present in the mouse NTS, and how information related to the N.IX and the N.X is integrated and processed to the higher-order sensory nuclei.

In conclusion, the present study revealed the onset of functional synaptic transmission in the N.IX-related neural circuits. The development of synaptic networks was temporally similar between the N.IX and the N.X, but was not spatially identical between the nerves or between rodents and birds. Multiple-site optical recordings and contour line maps presented here represent the locations and extent of the sensory nuclei at the early stages of nuclear organization. At these stages, morphological differentiation of the brain is immature, and anatomical boundaries of the nuclei are difficult to identify (Schambra, 2008). The present study demonstrated that optical recording with the VSD is a powerful tool to investigate developmental organization of the brainstem nuclei and functiogenesis of neural circuits during the early phase of ontogenesis.

Author contributions

YMS designed and performed experiments. YMS and KS analyzed data and prepared the manuscript.

Conflicts of interest

There is no conflicts of interest to disclose concerning this study.

Acknowledgements

This research was supported by grants from the Ministry of Education, Culture, Sports, Science and Technology of Japan (15K06720, 18K06530, 19K06962) and Opto-Medical Institute.

References

Abadie, V., Champagnat, J., Fortin, G., 2000. Brachiomotor activities in mouse embryo. Neuroreport 11, 141–145.
Altman, J., Bayer, S.A., 1980. Development of the brain stem in the rat. I. Thymidine-radiographic study of the time of origin of neurons of the lower medulla. J. Comp. Neurol. 194, 1–35.
Altman, J., Bayer, S.A., 1982. Development of the Cranial Nerve Ganglia and Related Nuclei in the Rat. Springer-Verlag, Berlin.
Baker, B.J., Kosmidis, E.K., Vucinic, D., Falk, C.X., Cohen, L.B., Djurisic, M., Zecevic, D., 2005. Imaging brain activity with voltage- and calcium-sensitive dyes. Cell. Mol. Neurobiol. 25, 245–282.
Beckmann, M.E., Whitehead, M.C., 1991. Intramedullary connections of the rostral nucleus of the solitary tract in the hamster. Brain Res. 557, 265–279.
Breazile, J.E., 1979. Systema nervosum central. In: Baumel, J.J., King, A.S., Lucas, A.M., Breazile, J.E., Evans, H.E. (Eds.), Nomina Anatomica Avium: An Annotated Anatomical Dictionary of Birds. Academic Press, New York, pp. 417–472.
Canepari, M., Zecevic, D., Bernus, O., 2015. Membrane Potential Imaging in the Nervous System and Heart. Springer, New York.
Carpenter, M.B., 1985. Core Text of Neuroanatomy, 3rd ed. Williams and Wilkins, Baltimore.
Chambers, D., Wilson, L.J., Alfonsi, F., Hunter, E., Saxena, U., Blanc, E., Lumsden, A., 2009. Rhombomere-specific analysis reveals the repertoire of genetic cues expressed across the developing hindbrain. Neural Dev. 4, 6.
Chédotal, A., Rijli, F.M., 2009. Transcriptional regulation of tangential neuronal migration in the developing forebrain. Cur. Opin. Neurobiol. 19, 139–145.
Cohen, L.B., Salzberg, B.M., 1978. Optical measurement of membrane potential. Rev. Physiol. Biochem. Pharmacol. 83, 35–88.
Dasheiff, R.M., 1988. Fluorescent voltage-sensitive dyes: applications for neurophysiology. J. Clin. Neurophysiol. 5, 211–235.
Ebner, T.J., Chen, G., 1995. Use of voltage-sensitive dyes and optical recordings in the central nervous system. Prog. Neurobiol. 46, 463–506.
Glover, J.C., Sato, K., Momose-Sato, Y., 2008. Using voltage-sensitive dye recording to image the functional development of neuronal circuits in vertebrate embryos. Dev. Neurobiol. 68, 804–816.
Grinvald, A., Frostig, R.D., Lieke, E., Hildesheim, R., 1988. Optical imaging of neuronal activity. Physiol. Rev. 68, 1285–1366.
Herbert, H., Moga, M.M., Saper, C.B., 1990. Connections of the parabrachial nucleus with the nucleus of the solitary tract and the medullary reticular formation in the rat. J. Comp. Neurol. 293, 540–580.
Hirota, A., Sato, K., Momose-Sato, Y., Sakai, T., Kamino, K., 1995. A new simultaneous 1020-site optical recording system for monitoring neural activity using voltage-sensitive dyes. J. Neurosci. Methods 56, 187–194.
Jacobowitz, D.M., Addott, L.C., 1997. Chemoarchitectonic Atlas of the Developing Mouse Brain. CRC Press, Boca Raton.
Kamino, K., 1991. Optical approaches to ontogeny of electrical activity and related functional organization during early heart development. Physiol. Rev. 71, 53–91.
Kamino, K., Hirota, A., Fujii, S., 1981. Localization of pacemaking activity in early embryonic heart monitored using voltage-sensitive dye. Nature 290, 595–597.
Kandel, E.R., Schwartz, J.H., Jessell, T.M., Siegelbaum, S.A., Hudspeth, A.J., 2013. Principles of Neural Science, 5th ed. McGraw-Hill, New York.
Komuro, H., Sakai, T., Momose-Sato, Y., Hirota, A., Kamino, K., 1991. Optical detection of postsynaptic potentials evoked by vagal stimulation in the early embryonic chick brain stem slice. J. Physiol. (Lond.) 442, 631–648.
Loew, L.M., 1988. How to choose a potentiometric membrane probe. In: In: Loew, L.M. (Ed.), Spectroscopic Membrane Probes Vol. II. CRC Press, Florida, pp. 139–151.
Mifflin, S.W., Felder, R.B., 1990. Synaptic mechanisms regulating cardiovascular afferent inputs to solitary tract nucleus. Am. J. Physiol. 259, H653–H661.
Miller, E.W., 2016. Small molecule fluorescent voltage indicators for studying membrane potential. Curr. Opin. Chem. Biol. 33, 74–80.
Momose-Sato, Y., Sato, K., 2006. Optical recording of vagal pathway formation in the embryonic brainstem. Auton. Neurosci.: Basic Clin. 126-127, 39–49.
Momose-Sato, Y., Sato, K., 2011. The embryonic brain and development of vagal pathways. Resp. Physiol. Neurobiol. 178, 163–173.
Momose-Sato, Y., Sato, K., 2016. Development of synaptic networks in the mouse vagal

pathway revealed by optical mapping with a voltage-sensitive dye. Eur. J. Neurosci. 44, 1906–1918.
Momose-Sato, Y., Sakai, T., Komuro, H., Hirota, A., Kamino, K., 1991. Optical mapping of the early development of the response pattern to vagal stimulation in embryonic chick brain stem. J. Physiol. (Lond.) 442, 649–668.
Momose-Sato, Y., Sakai, T., Hirota, A., Sato, K., Kamino, K., 1994. Optical mapping of early embryonic expression of Mg^{2+}-/APV-sensitive components of vagal glutaminergic EPSPs in the chick brainstem. J. Neurosci. 14, 7572–7584.
Momose-Sato, Y., Sato, K., Sakai, T., Hirota, A., Matsutani, K., Kamino, K., 1995. Evaluation of optimal voltage-sensitive dyes for optical monitoring of embryonic neural activity. J. Memb. Biol. 144, 167–176.
Momose-Sato, Y., Sato, K., Kamino, K., 2001. Optical approaches to embryonic development of neural function in the brainstem. Prog. Neurobiol. 63, 151–197.
Momose-Sato, Y., Sato, K., Kamino, K., 2002. Application of voltage-sensitive dyes to the embryonic central nervous system. In: In: Fagan, J., Davidson, J.N., Shimizu, N. (Eds.), Recent Research Developments in Membrane Biology Vol. 1. Research Signpost, Kerala, pp. 159–181.
Momose-Sato, Y., Kinoshita, M., Sato, K., 2007. Embryogenetic expression of glossopharyngeal and vagal excitability in the chick brainstem as revealed by voltage-sensitive dye recording. Neurosci. Lett. 423, 138–142.
Momose-Sato, Y., Nakamori, T., Sato, K., 2011. Functional development of the vagal and glossopharyngeal nerve-related nuclei in the embryonic rat brainstem: optical mapping with a voltage-sensitive dye. Neuroscience 192, 781–792.
Momose-Sato, Y., Nakamori, T., Mullah, S.H.-E.-R., Sato, K., 2013. Optical survey of vagus nerve-related neuronal circuits in the embryonic rat brainstem. Neurosci. Lett. 535, 140–145.
Momose-Sato, Y., Sato, K., Kamino, K., 2015. Monitoring population membrane potential signals during development of the vertebrate nervous system. In: Canepari, M., Zecevic, D., Bernus, O. (Eds.), Membrane Potential Imaging in the Nervous System and Heart. Springer, New York, pp. 213–242.
Mullah, S.H.-E.-R., Komuro, R., Yan, P., Hayashi, S., Inaji, M., Momose-Sato, Y., Loew, L.M., Sato, K., 2013. Evaluation of voltage-sensitive fluorescence dyes for monitoring neuronal activity in the embryonic central nervous system. J. Memb. Biol. 246, 679–688.
Norgen, R., 1978. Projections from the nucleus of the solitary tract in the rat. Neuroscience 3, 207–218.
Norgen, R., Leonard, C.M., 1973. Ascending central gustatory pathways. J. Comp. Neurol. 150, 217–238.
Obaid, A.L., Orkand, R.K., Gainer, H., Salzberg, B.M., 1985. Active calcium responses recorded optically from nerve terminals of the frog neurohypophysis. J. Gen. Physiol. 85, 481–489.
Orbach, H.S., Cohen, L.B., Grinvald, A., 1985. Optical mapping of electrical activity in rat somatosensory and visual cortex. J. Neurosci. 5, 1886–1895.
Paton, J.F.R., Kasparov, S., 2000. Sensory channel specific modulation in the nucleus of the solitary tract. J. Auton. Nerv. Syst. 80, 117–129.
Ross, W.N., Salzberg, B.M., Cohen, L.B., Grinvald, A., Davila, H.V., Waggoner, A.S., Wang, C.H., 1977. Changes in absorption, fluorescence, dichroism, and birefringence in stained giant axons: optical measurement of membrane potential. J. Memb. Biol. 33, 141–183.
Sajgo, S., Ali, S., Posescu, O., Badea, T.C., 2016. Dynamic expression of transcription factor Brn3b during mouse cranial nerve development. J. Comp. Neurol. 524, 1033–1061.
Salzberg, B.M., 1983. Optical recording of electrical activity in neurons using molecular probes. In: Barker, J.L., McKelvy, J.F. (Eds.), Current Methods in Cellular Neurobiology, Vol. 3. Electrophysiological Techniques. Wiley, New York, pp. 139–187.
Salzberg, B.M., Obaid, A.L., Senseman, D.M., Gainer, H., 1983. Optical recording of action potentials from vertebrate nerve terminals using potentiometric probes provides evidence for sodium and calcium components. Nature 306, 36–40.
Sato, K., Momose-Sato, Y., 2004a. Optical mapping reveals developmental dynamics of Mg^{2+}-/APV-sensitive components of glossopharyngeal glutamatergic EPSPs in the embryonic chick NTS. J. Neurophysiol. 92, 2538–2547.
Sato, K., Momose-Sato, Y., 2004b. Optical detection of convergent projections in the embryonic chick NTS. Neurosci. Lett. 371, 97–101.
Sato, K., Momose-Sato, Y., 2017. Functiogenesis of the embryonic central nervous system revealed by optical recording with a voltage-sensitive dye. J. Physiol. Sci. 67, 107–119.
Sato, K., Momose-Sato, Y., Sakai, T., Hirota, A., Kamino, K., 1995. Responses to glossopharyngeal stimulus in the early embryonic chick brainstem: spatiotemporal patterns in three dimensions from repeated multiple-site optical recording of electrical activity. J. Neurosci. 15, 2123–2140.
Sato, K., Momose-Sato, Y., Hirota, A., Sakai, T., Kamino, K., 1998. Optical mapping of neural responses in the embryonic rat brainstem with reference to the early functional organization of vagal nuclei. J. Neurosci. 18, 1345–1362.
Sato, K., Mochida, H., Sasaki, S., Momose-Sato, Y., 2002a. Developmental organization of the glossopharyngeal nucleus in the embryonic chick brainstem slice as revealed by optical sectioning recording. Neurosci. Lett. 327, 157–160.
Sato, K., Mochida, H., Yazawa, I., Sasaki, S., Momose-Sato, Y., 2002b. Optical approaches to functional organization of glossopharyngeal and vagal motor nuclei in the embryonic chick hindbrain. J. Neurophysiol. 88, 383–393.
Sato, K., Miyakawa, N., Momose-Sato, Y., 2004. Optical survey of neural circuit formation in the embryonic chick vagal pathway. Eur. J. Neurosci. 19, 1217–1225.
Schambra, U., 2008. Prenatal Mouse Brain Atlas. Springer, New York.
Simon, H., Lumsden, A., 1993. Rhombomere-specific origin of the contralateral vestibuloacoustic efferent neurons and their migration across the embryonic midline. Neuron 11, 209–220.
Sissman, N.J., 1970. Developmental landmarks in cardiac morphogenesis: comparative chronology. Am. J. Cardiol. 25, 141–148.
Travers, J.B., 1988. Efferent projections from the anterior nucleus of the solitary tract of the hamster. Brain Res. 457, 1–11.
Tsytsarev, V., Liao, L.-D., Kong, K.V., Liu, Y.-H., Erzurumlu, R.S., Olivo, M., Thakor, N.V., 2014. Recent progress in voltage-sensitive dye imaging for neuroscience. J. Nanosci. Nanotechnol. 14, 4733–4744.
Watari, N., Kameda, Y., Takeichi, M., Chisaka, O., 2001. Hoxa3 regulates integration of glossopharyngeal nerve precursor cells. Dev. Biol. 240, 15–31.
Watson, C., Paxinos, G., Puelles, L., 2012. The Mouse Nervous System. Elsevier, London.
Whitehead, M.C., 1990. Subdivisions and neuron types of the nucleus of the solitary tract that project to the parabrachial nucleus in the hamster. J. Comp. Neurol. 301, 554–574.
Whitehead, M.C., 1993. Distribution of synapses on identified cell types in a gustatory subdivision of the nucleus of the solitary tract. J. Comp. Neurol. 332, 326–340.
Zaidi, F.N., Todd, K., Enquist, L., Whitehead, M.C., 2008. Types of taste circuits synaptically linked to a few geniculate ganglion neurons. J. Comp. Neurol. 511, 753–772.